Structure and short-time dynamics in suspensions of charged silica spheres in the entire fluid regime

J. Gapinski, A. Patkowski, A. J. Banchio, J. Buitenhuis, P. Holmqvist et al.

Citation: J. Chem. Phys. **130**, 084503 (2009); doi: 10.1063/1.3078408
View online: http://dx.doi.org/10.1063/1.3078408
View Table of Contents: http://jcp.aip.org/resource/1/JCPSA6/v130/i8
Published by the AIP Publishing LLC.

Structure and short-time dynamics in suspensions of charged silica spheres in the entire fluid regime

J. Gapinski,[1,a)] A. Patkowski,[1] A. J. Banchio,[2] J. Buitenhuis,[3] P. Holmqvist,[3] M. P. Lettinga,[3] G. Meier,[3] and G. Nägele[3]
[1]*Faculty of Physics, A. Mickiewicz University, 61-614 Poznan, Poland*
[2]*CONICET and FaMAF, Universidad Nacional de Córdoba, Ciudad Universitaria, X5000HUA Córdoba, Argentina*
[3]*Institut für Festkörperforschung, Forschungszentrum Jülich, D-52425 Jülich, Germany*

(Received 6 November 2008; accepted 15 January 2009; published online 27 February 2009)

We present an experimental study of short-time diffusion properties in fluidlike suspensions of monodisperse charge-stabilized silica spheres suspended in dimethylformamide. The static structure factor $S(q)$, the short-time diffusion function $D(q)$, and the hydrodynamic function $H(q)$ have been probed by combining x-ray photon correlation spectroscopy experiments with static small-angle x-ray scattering. Our experiments cover the full liquid-state part of the phase diagram, including de-ionized systems right at the liquid-solid phase boundary. We show that the dynamic data can be consistently described by the renormalized density fluctuation expansion theory of Beenakker and Mazur over a wide range of concentrations and ionic strengths. In accordance with this theory and Stokesian dynamics computer simulations, the measured short-time properties cross over *monotonically*, with increasing salt content, from the bounding values of salt-free suspensions to those of neutral hard spheres. Moreover, we discuss an upper bound for the hydrodynamic function peak height of fluid systems based on the Hansen–Verlet freezing criterion. © *2009 American Institute of Physics*. [DOI: 10.1063/1.3078408]

I. INTRODUCTION

Dispersions of charge-stabilized colloidal particles are ubiquitous in environmental and food industry and in life sciences. Examples of such dispersions are viruses or proteins in water, paints, waste water, and model systems of strongly charged spherical latex or silica spheres. The exploration of dynamic properties in these model systems provides insight into the transport properties of more complex colloidal or macromolecular suspensions. The dynamics of model systems of charged spheres (CSs) is the subject of ongoing experimental and theoretical research (see Refs. 1–4).

At long distances, charged colloidal spheres interact electrostatically by an exponentially screened Coulomb repulsion, originating from the overlap of electric double layers formed by surface-released counterions and salt ions. Colloidal particles also influence each other through solvent-mediated hydrodynamic interactions (HIs) which, in unconfined suspensions of mobile particles, are very long ranged.

In dynamic scattering experiments, one distinguishes between the colloidal short-time and colloidal long-time regimes. The present article is concerned with the short-time regime where only tiny changes in the particle configuration are probed. We report on a detailed experimental study of static and short-time diffusion properties in suspensions of very monodisperse, charged silica spheres suspended in dimethylformamide (DMF). Using the synchrotron radiation facility at the ESRF in Grenoble, we have performed x-ray photon correlation spectroscopy (XPCS) experiments to explore very systematically the concentration and ionic-strength dependence of the static structure factor $S(q)$, of short-time diffusion properties including the short-time diffusion function $D(q)$, and the related hydrodynamic function $H(q)$ as a function of the scattering wave number q. Our study encompasses the liquid phase regime. In particular, the fluid regime close to the liquid-solid phase boundary is explored.

We use DMF rather than water as the suspending solvent to avoid the problem of CO_2 adsorption and to cover the most interesting regime of very low salt concentrations where the colloids are still fluidlike ordered but close to the freezing into a crystal phase. Regarding the peak height in $H(q)$, our experiments bridge the gap between hard-sphere-like systems and fully de-ionized systems of strongly charged colloidal particles. The majority of earlier work was concerned with systems showing peak heights in $H(q)$ not far from the corresponding equal-concentration hard-sphere values.[5,6] In some earlier work, strikingly low peak values of $H(q)$ have been reported to occur in dense low-salt systems,[7–10] an observation which was interpreted initially in terms of hydrodynamic screening.[11]

We show that all our experimental short-time diffusion data, obtained for three different series of samples, can be consistently explained by the renormalized density fluctuation expansion method of Beenakker and co-workers,[12–14] referred to as the $\delta\gamma$-scheme. The scheme includes many-body HI in an approximate way. It is the most comprehensive analytical scheme available so far to calculate short-time dynamic properties. Originally, it had been applied to hard

[a)]Author to whom correspondence should be addressed. Electronic mail: gapinski@amu.edu.pl.

spheres (HSs) only, but in later work its zeroth-order version was used to make predictions also for charge-stabilized systems.[3,7,11,15–19] It requires the static structure factor as input, which we calculate using the Rogers–Young (RY) and rescaled mean-spherical approximation (RMSA) integral equation schemes.[20,21] The colloid pair interactions are described in these calculations on the basis of the one-component macroion fluid (OMF) model of dressed spherical macroions that interact by an effective screened Coulomb potential of Derjaguin–Landau–Verwey–Overbeek (DLVO) type. In recent accelerated Stokesian dynamics (ASD) computer simulation studies, we have shown that the $\delta\gamma$-scheme allows for the prediction of short-time diffusion properties on a semiquantitative level.[6,22–25]

In the present paper, we have achieved a thorough experimental test of the $\delta\gamma$-scheme by measuring simultaneously the short-time diffusion function and the static structure for each individual sample. For all samples considered, there has been no indication of unusually small values of $H(q)$ that would conflict with the standard predictions for the hydrodynamic function made by the $\delta\gamma$ theory and the ASD simulations.

The paper is organized as follows. Sec. II summarizes the theoretical background and explains our OMF model calculations. Experimental details on the silica in DMF system and the experimental methods and setup are provided in Sec. III. Section IV includes the discussion of our experimental results and the comparison with theory. Our conclusions are contained in Sec. V.

II. THEORY

A. Short-time dynamics

In dynamic scattering experiments on colloidal spheres, the dynamic structure factor

$$S(q,t) = \left\langle \frac{1}{N} \sum_{l,j=1}^{N} \exp\{i\mathbf{q} \cdot [\mathbf{r}_l(t) - \mathbf{r}_j(0)]\} \right\rangle \tag{1}$$

is probed. Here, N is the number of spheres in the scattering volume, $\boldsymbol{r}_j(t)$ is the vector pointing to the center of the jth colloidal sphere at time t, $\boldsymbol{q}$ is the scattering wave vector, and $\langle \ldots \rangle$ denotes an equilibrium ensemble average. At short correlation times, $S(q,t)$ decays exponentially according to[2,3]

$$\frac{S(q,t)}{S(q)} \approx \exp[-q^2 D(q) t], \tag{2}$$

with the short-time diffusion function $D(q)$. Application of the generalized Smoluchowski equation leads to the well-known expression[3]

$$D(q) = D_0 \frac{H(q)}{S(q)}, \tag{3}$$

relating $D(q)$ to the hydrodynamic function $H(q)$ and to the static structure factor $S(q)=S(q,t=0)$. Here, $D_0 = k_B T/(6\pi\eta_0 a)$ is the free diffusion coefficient at infinite dilution, a is the hydrodynamic sphere radius, and η_0 denotes the solvent shear viscosity. Thus, the hydrodynamic function can be determined from combing a short-time XPCS experiment for $D(q)$ with a small-angle x-ray scattering (SAXS) measurement of $S(q)$. The microscopic expression for $H(q)$ is[26]

$$H(q) = \left\langle \frac{k_B T}{N D_0} \sum_{l,j=1}^{N} \hat{\mathbf{q}} \cdot \mu(\mathbf{r}^N)_{lj} \cdot \hat{\mathbf{q}} \exp[i\mathbf{q} \cdot (\mathbf{r}_l - \mathbf{r}_j)] \right\rangle, \tag{4}$$

where $\hat{\mathbf{q}}$ is the unit vector along the direction of $\mathbf{q}$ and the $\mu(\mathbf{r}^N)_{lj}$ are the hydrodynamic mobility tensors relating a force on sphere j to the resulting velocity of sphere l. The mobility tensors depend on the positions $\mathbf{r}^N$ of all N particles. This makes an analytic calculation of $H(q)$ intractable, so that approximations have to be introduced.

The function $H(q)$ contains the influence of the HI on the short-time diffusion. It is the sum of a q-independent self-part and a q-dependent distinct part,

$$H(q) = \frac{D_s}{D_0} + H_d(q), \tag{5}$$

where D_s is the short-time translational self-diffusion coefficient. Without HI, $H(q)$ is equal to one for all values of q. Any variation in its dependence on the scattering wave number is thus indicative of the influence of HI.

B. Nonhydrodynamic interactions

The calculation of $H(q)$ and $S(q)$ in this work is based on the OMF model. This model describes the colloidal particles as uniformly charged HSs interacting by an effective pair potential of DLVO-type[27]

$$\frac{u(r)}{k_B T} = L_B Z^2 \left(\frac{e^{\kappa a}}{1+\kappa a} \right)^2 \frac{e^{-\kappa r}}{r}, \quad r > 2a. \tag{6}$$

For the closed systems studied here, the electrostatic screening parameter κ is given by

$$\kappa^2 = \frac{4\pi L_B [n|Z| + 2n_s]}{1-\phi} = \kappa_{\mathrm{ci}}^2 + \kappa_s^2, \tag{7}$$

where n is the colloid number density, n_s is the number density of added 1-1 electrolyte, and $\phi=(4\pi/3)na^3$ is the colloid volume fraction. Furthermore, Z is the (effective) charge on a colloid sphere in units of the elementary charge e and $L_B = e^2/(\varepsilon k_B T)$ is the Bjerrum length for a suspending fluid of dielectric constant ε at temperature T. We note that κ^2 is the sum of a contribution κ_{ci}^2 due to surface-released counter ions, which are monovalent for silica spheres in DMF, and a contribution κ_s^2 arising from the added 1-1 electrolyte, which is LiCl in our case. The factor $1/(1-\phi)$ corrects for the free volume accessible to the microions.[28,29]

For strongly CSs where $L_B|Z|/a > 1$, the value of Z in Eq. (6) needs to be interpreted as an effective or renormalized charge number smaller than the bare one to account to some extent for the nonlinear electrostatic screening close to the colloid surface caused by quasicondensed counterions. Likewise, a renormalized value for κ must be used. Several approximate schemes have been developed to relate the effective Z and κ to the bare ones.[30–36] The outcome of these schemes depends on the approximation made for the free

energy functional and on additional simplifying model assumptions such as the usage of a spherical cell[37,38] or the spherical jellium model description.[35]

There is an ongoing discussion on how the effective charge and screening parameters in the effective pair potential are related to their bare counterparts and under what conditions three-body and higher-order corrections to the OMF pair potential come into play. Even though promising advances have been made, this remains as a challenging many-particle problem, in particular, for low-salinity systems with strongly overlapping electric double layers. Since our major concern is about short-time dynamic properties, we use the OMF model as a well-defined and well-established model that certainly captures essential features of charge-stabilized suspensions, thus allowing to study general trends in the short-time dynamic properties. However, in Sec. IV C, we shall discuss on a qualitative level the salt and colloid concentration dependence of the effective charge Z, as obtained from a static structure factor fit procedure explained below, and we compare it with our findings for the electrophoretic colloid charge and the renormalized colloid charge obtained from a renormalized jellium model (RJM) calculation.

Analytic calculations of short-time properties based on the $\delta\gamma$ scheme require as input the colloidal static structure factor $S(q)$, for which we use the RY and RMSA integral equation schemes.[3,20,21,39] The RY scheme is known for its excellent structure factor predictions for fluid systems of Yukawa-like particles. The RMSA results for $S(q)$ are in most cases nearly identical to the RY predictions, provided a somewhat different and usually larger value of Z is used. RMSA calculations are very fast and can be efficiently used for extensive structure factor scans.

C. Method of calculation

A comprehensive analytic method that allows to predict the hydrodynamic function of dense suspensions of charge-stabilized or neutral HSs is the (zeroth order) $\delta\gamma$-scheme of Beenakker and Mazur.[12] It is based on a partial resummation of the many-body HI contributions. According to this scheme, $H(q)$ is obtained to leading order in the renormalized density fluctuations from[12,15]

$$H_d(q) = \frac{3}{2\pi}\int_0^\infty d(ak)\left(\frac{\sin(ak)}{ak}\right)^2 [1+\phi S_{\gamma 0}(ak)]^{-1} \times \int_{-1}^{1} dx(1-x^2)[S(|q-k|)-1] \quad (8)$$

and

$$\frac{D_s(\phi)}{D_0} = \frac{2}{\pi}\int_0^\infty dx\left(\frac{\sin x}{x}\right)^2 [1+\phi S_{\gamma 0}(x)]^{-1}, \quad (9)$$

where x is the cosine of the angle extended by the wave vectors $\mathbf{q}$ and $\mathbf{k}$ and $S_{\gamma 0}(x)$ is a known function independent of the particle correlations and given in Refs. 12 and 15. The only input is the static structure factor $S(q)$, which we calculate using the RY and RMSA integral equation schemes. $S(q)$ enters only into the distinct part of $H(q)$ since, to lowest order in the renormalized density fluctuations expansion, the self-part is independent of $S(q)$. For CSs, the short-time self-diffusion coefficient is thus more roughly approximated by the value for neutral HSs at the same ϕ, independent of the sphere charge and screening parameter. To include the actual pair correlations into the calculation of D_s requires to go one step further in the fluctuating density expansion, which severely complicates the scheme. Yet, a detailed comparison of the $\delta\gamma$-scheme predictions with ASD simulations and experimental data on charge-stabilized systems has shown that $H_d(q)$ is, in general, well captured by Eq. (8). This observation allows to improve the $\delta\gamma$ scheme through replacing the $\delta\gamma$-D_s by a more accurate simulation prediction, which is computationally less expensive than a full simulation of $H(q)$. Even without an improved input for D_s, the $\delta\gamma$ scheme remains useful in predicting general trends in the behavior of $H(q)$ on a semiquantitative level of accuracy. The analytic simplicity of the $\delta\gamma$-scheme has allowed us in the present work to interpret theoretically a comprehensive set of short-time diffusion data for a wide range of system parameters.

III. MATERIALS AND EXPERIMENTAL METHODS

A. Sample characterization

In the present series of experiments, we use uncoated silica particles dispersed in DMF. Monodisperse silica seed particles with a hydrodynamic radius of 27 nm were synthesized in a microemulsion.[40,41] These seed particles were grown to their final size by seeded growth with continuous addition of monomer according to Giesche.[42] The final sample was redispersed in DMF. The solvent DMF was purchased from Sigma (CHROMASOLV Plus, for HPLC, $\geq$99.9%). A refractive index of $n=1.428$, mass density of $\rho_{\mathrm{DMF}}=0.944$ g/cm^3, shear viscosity $\eta_0(\mathrm{DMF})=0.92$ cP, and dielectric constant $\varepsilon_{\mathrm{DMF}}=36.7$ at 20 °C were used for DMF to calculate the hydrodynamic radius (from a dynamic light scattering measurement), the colloid volume fraction, and the Debye screening length. For the silica particles, a mass density of $\rho_s=1.95$ g/cm^3 was assumed for further calculations. The batch suspension of silica particles in DMF was prepared by performing multiple sequences of operations including the centrifugation of a dilute sample at 1000 g for 10 h, the exchange of the supernatant with pure DMF, and a subsequent redispersion. In the final step of the preparation, the supernatant was removed to such a level that the colloid weight concentration of the suspension was 0.35 g/g. The silica particles were then resuspended by intensive mechanical mixing.

Transmission electron microscopy gave an average particle radius of 80.5 nm with a relative standard deviation of the size distribution smaller than 2%. For comparison, the hydrodynamic radius of the spheres as measured by dynamic light scattering in a very dilute DMF suspension amounts to 87.7 nm. The radius determined from the form factor measurement in dilute DMF suspensions using SAXS and a homogeneous-sphere form factor fit is 85.5 nm, again with a size polydispersity smaller than 2%. The differences between

these various particle radii are, in fact, rather small in comparison to the differences found in some other silica dispersions.[43]

To control the ionic strength, we added controlled amounts of a lithium chloride (LiCl, Sigma, ≥99%) solution in DMF (200 mM batch solution).

In our x-ray scattering experiments, the samples were filled into quartz capillaries of a diameter of 1.5 mm (0.01 mm wall thickness) and sealed with glue.

B. Experimental methods

The x-ray scattering experiment was performed at the Troïka III part of the ID10A beamline of the European Synchrotron Radiation Facility (ESRF) in Grenoble. The experimental details concerning the beam characteristics and the general setup have been given elsewhere[6,44] and can also be found on the ESRF web page.[45] We took advantage of the uniform filling mode of the synchrotron which allowed us to avoid the problem of oscillations in the correlation functions.[44] The average current of the beam was about 200 mA. For all the measurements, we utilized radiation of the wavelength of 1.55 Å, which corresponds to a photon energy of 7.99 keV.

The size of the pinhole placed 25 cm in front of the sample was a compromise between the need for high flux (10^9 photons/s/100 mA) and the beam coherence. For the XPCS measurements, it was reduced to 12 μm, while for the SAXS scans it could be opened to twice this value. The capillary containing the sample was mounted in a chamber connected to a long pipe guiding the scattered photons to the detector placed at the distance of 3.480 m from the sample. Both the chamber and the pipe were evacuated. The two slits (vertical and horizontal) in front of the detector (Bicron scintillation counter) were closed to 150 μm to provide a reasonable coherent and unsmeared detection of scattered radiation in the XPCS measurements. For the SAXS scans the vertical size of the detector window was usually increased to about 300 μm. Time correlation functions were calculated using an ALV-6000 digital correlator (ALV GmbH, Langen).

Electrophoresis measurements were performed on a Malvern Zetasizer 2000. With this apparatus, we have measured the electrophoretic mobility of silica dispersions in DMF at 25 °C as a function of the LiCl concentration, and for a particle concentration of 2.5 g/l, corresponding to a volume fraction of about 1.25×10^{-3}. The measurements were repeated several times to check for the reproducibility of the results.

IV. RESULTS AND DISCUSSION

In the following, we discuss our experimental results for the static and short-time diffusion properties of fluidlike suspensions of silica spheres in DMF (at fixed temperature $T=20$ °C). We investigated three distinct series of samples labeled as H, K, and C, respectively. All parameters characterizing these series are summarized in Table I. In the first two series, H and K, the weight concentration C_w quantifying the weight of silica spheres relative to that of the whole suspension was fixed to 150 and 250 mg/g, respectively, while the concentration C_s of added LiCl was varied. In the less concentrated samples of series H, C_s was varied from 0–20 mM, while C_s was varied from 70–400 μM in the more concentrated samples of series K. Series C consists of samples with fixed salinity $C_s=50$ μM with the weight concentration of silica spheres varied from 100 to 200 mg/g. For all samples in the table, we have inspected by eye that there is no indication of crystallization in the form of iridescent light. In series H, some traces of crystallization were recognized by the appearance of crystal-like peaks in the SAXS scattering function within the added salt region of 5–10 μM. In series K, a reduction in the salt concentration below 70 μM resulted in the crystallization of the samples.

In the present paper, systems indicative of (partial) crystallization have been excluded from the analysis and from Table I, since our focus here is on liquid-like samples. The XPCS analysis of the dynamics in (partially) crystalline samples requires a special analysis different from that for liquid-like systems. This will be discussed in the forthcoming paper.

The effective charge numbers, Z_{RY} and Z_{RMSA}, have been deduced by fitting the peak height of the RY and RMSA $S(q)$ to the experimental one. The experimental structure factors (in Figs. 2–4) were first fitted using the very efficient RMSA code. In the second step, the more elaborate and less time-efficient RY code was applied to fit the structure factor peaks by adjusting Z_{RY}, with Z_{RMSA} providing an upper limit to the actual charge number. It is well known that the RMSA values for the effective charge are in most cases somewhat larger than the more accurate RY ones, reflecting the tendency of the RMSA to underestimate static pair correlations. A small readjustment of the volume fraction ϕ of silica spheres in the samples of series H and K was required for a nearly perfect match of the wave number position of the RY and RMSA structure factor peaks to the experimental one. This is the reason for the small variation in ϕ values in the table of series H and K. Aside from this slight readjustment, the effective charge has been the only adjustable parameter. The values for the screening parameter κ were obtained using Eq. (7) in combination with the RY value of the effective charge.

As we have found by visual inspection, there is a broad range of colloid and salt ion concentrations where the silica samples crystallize at least partially. Since we study here fluidlike samples, we carefully selected rather two high volume fractions of silica spheres, namely, those of series H and K given, respectively, by $\phi\approx0.07-0.08$ and $\phi\approx0.13-0.14$. This has allowed us to scan a broad range of added salt concentrations while having samples in the fluid state. In this way, we could tune the electrostatic interactions from being practically screened out to very strong values for a single fixed colloid concentration.

A. Form factor

Figure 1 shows our SAXS measurements of the mean scattered intensity in a broad range of wave numbers q, for a silica-sphere suspension of moderate concentration of 150 mg/ml, and in presence of 100 μM added LiCl. Under the

TABLE I. Parameters used in the $\delta\gamma$-scheme calculations of $H(q)$ and $D(q)$. The solvent is DMF at $T=20$ °C and $\varepsilon=36.7$, corresponding to a Bjerrum length $L_B=1.554$ nm. The radius $a=85.5$ nm obtained from the form factor measurement was used in all our calculations. The values for the effective charge Z were obtained from fitting the peak values of the RY and RMSA-$S(q)$, respectively, to the experimental ones (see Figs. 2–4). Three different series of samples have been studied. The samples in series H and K are for a fixed particle concentration but varying salinity, whereas in series C the salinity is fixed and the silica concentration is varied: ϕ-silica volume fraction; C_w-silica weight concentration in mg/g; C_s—added LiCl concentration, Z_{RMSA}, and Z_{RY}—effective charge numbers, in units of elementary charge e, obtained, respectively, from the RMSA and RY structure factor peak height fits; and κ-inverse screening length calculated using Z_{RY}. Z_{el}—effective charge number deduced from electrophoresis measurements on dilute samples ($\phi=1.25\times10^{-3}$). The missing input in the table for $C_s=20$ mM is due to the fact that for such a high amount of salt the peak height of $S(q)$ is quite insensitive to Z.

Sample	ϕ	C_w (mg/g)	Z_{RMSA} (e)	Z_{RY} (e)	Z_{el} (e)	κ (nm^{-1})	κa
C_s (μM)			Series H $C_w=150$ mg/g				
0	0.0795	150	220	177	383	0.0108	0.923
20	0.0744	142	350	282	845	0.0260	2.22
50	0.0718	137	600	520	895	0.0396	3.38
100	0.0769	146	1000	900	928	0.0557	4.76
200	0.0820	155	5000	3500	1036	0.0864	7.39
20 000	0.0769	146	⋯	⋯	2552	>0.686	>58.6
C_s (μM)			Series K $C_w=250$ mg/g				
70	0.131	236	1600	850	⋯	0.0534	4.56
100	0.131	236	2500	1700	928	0.0679	5.80
150	0.131	236	3000	2200	⋯	0.0808	6.91
200	0.136	236	4000	4000	1036	0.101	8.64
400	0.136	236	5000	3500	⋯	0.122	10.4
C_w (mg/g)			Series C $C_s=50$ μM				
100	0.0564	109	900	790	895	0.0400	3.42
150	0.0718	137	600	520	895	0.0396	3.38
200	0.108	198	380	320	895	0.0401	3.43

conditions of this experiment, the structure factor levels off at the value of 1 within the experimental errors, already for $q>0.08$, which thus defines the region where $I(q)\cong P(q)$. The experimental points were scaled to match the theoretical form factor curve $P(q)$ for a Gaussian diameter distribution of homogeneous spheres of mean radius 85.5 nm and a relative standard deviation of 1%. The presence of multiple, sharp minima is a clear indication of a very low size polydispersity, quantified by the small value of 1% for the relative standard deviation in the calculated $P(q)$.

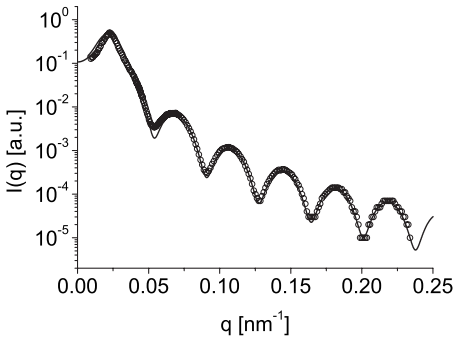

FIG. 1. SAXS result for the normalized mean scattered intensity obtained for silica spheres in DMF at the concentration of 150 mg/ml and with 100 μM added LiCl (open circles). The solid line represents the calculated intensity $I(q)=S(q)P(q)$. The form factor $P(q)$ was calculated for a Gaussian size distribution of homogeneously scattering spheres of mean radius 85.5 nm and relative standard deviation of 1%.

B. Structure factor and short-time diffusion properties

For each sample, a static SAXS measurement was performed for an extended number of scattering wave numbers in order to identify the position and height of the static structure factor peak. The analysis of the SAXS data to deduce $S(q)$ from the measured mean intensity included a correction for the q-dependent background obtained for pure DMF. After this background correction, the system parameters were determined from matching the shape of the product function of the RY or RMSA, $S(q)$ and $P(q)$, to the background-corrected experimental intensity data for the full range of experimental q values.

In the XPCS measurements of the scattered radiation intensity autocorrelation function $g^{(2)}(q,t)$, 6–12 q-values out of a set of wave numbers probed in the SAXS experiments were selected. Then, using the Siegert relation, the first-order correlation function $g^{(1)}(q,t)$ was calculated and analyzed in terms of the (short-time) initial slope $\Gamma_i(q)$ of $\ln g^{(1)}(q,t)$. The values for the short-time diffusion function were obtained from $D(q)=\Gamma_i(q)/q^2$ and then normalized by the value $D_0=2.72\times10^{-8}$ cm^2/s for the free diffusion coefficient of a single silica sphere obtained from a light scattering PCS experiment.

In Figs. 2–4, we have plotted the reciprocal of the normalized diffusion function $D_0/D(q)$, rather than $D(q)$ itself. This allows for a direct comparison with the data for $S(q)$

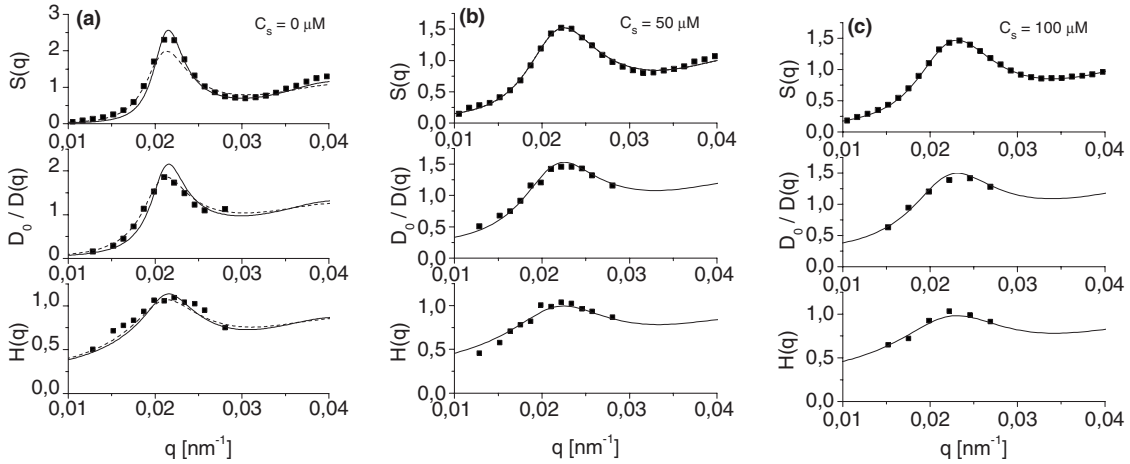

FIG. 2. [(a)–(c)] Results for $S(q)$, $H(q)$, and the reciprocal of the normalized $D(q)$ obtained for the fixed colloid concentration samples of series H. The filled symbols are the data from the combined SAXS and XPCS measurements. The lines are RY-fit results of $S(q)$ and the $\delta\gamma$-scheme results for $H(q)$ and $D(q)$ based on the fitted $S(q)$ input. The dashed lines for $S(q)$ and $H(q)$ in (a) are the RY and $\delta\gamma$-scheme results obtained when the peak height of the experimental diffusion function $D(q)$ is fitted instead of the peak in $S(q)$ (see text for details). All system parameters used in the calculations are listed in Table I. Additional results on the series H are available in the supplementary material (Ref. 46) in Fig. S1.

since $D_0/D(q)$ reduces to the static structure factor for negligible HI. Therefore, any observed difference in the two functions indicates the influence of HI. The experimental points for $H(q)$ were obtained from multiplying the experimental $D(q)/D_0$ by the peak-height fitted RY-$S(q)$ instead of the experimental points to avoid progression of statistical errors in the data. This procedure is justified since for all samples considered in Figs. 2–4, the RY-$S(q)$ is a decent description of the experimental structure factors. The $\delta\gamma$-scheme results for $H(q)$ shown in the figures have been calculated using the peak-height-fitted $S(q)$.

Figure 2 includes a summary of results for the samples of series H obtained from the SAXS measurements of $S(q)$ and the XPCS measurements of $D(q)$. The concentrations of added salt are indicated on the upper right corner of the plots. Additionally shown is the hydrodynamic function $H(q)$, as obtained from the experimental data for $D(q)$, by using Eq. (3) (symbols), and from $\delta\gamma$-scheme calculations (lines). In the low-salt region of series H in between 5–10 μM, which we have explored also experimentally, we find some traces of crystallization. In particular, for $C_s = 5$ μM, the measured intensity contained crystal-like peaks and, thus, could not be well fitted using the RY and RMSA integral schemes, which are designed to describe the fluid state only. Therefore these data are not used. While the zero-salinity sample ($C_s = 0$ μM) in series H appears to be fluid-like and has been therefore included into Table I, it cannot be excluded that it is partially crystalline. In fact, if instead of $S(q)$ one alternatively fits the peak height of the $\delta\gamma\, D(q)$ to the experimental diffusion function, the resulting $S(q)$ turns out to be less structured than the experimental one [see the dashed lines in Fig. 2(a)], indicating that there are probably some additional intensity contributions to the structure factor peak that arises from partially crystalline order.

Due to the dissociation-association mass action equilibrium of the silanol (SiOH) groups on the silica surfaces, the number of surface charges (i.e., SiO^- groups) can decrease with decreasing salt concentration.[1,47] Nevertheless, the effect of the larger electrostatic screening length dominates for very small values of C_s causing (partial) crystallization. This

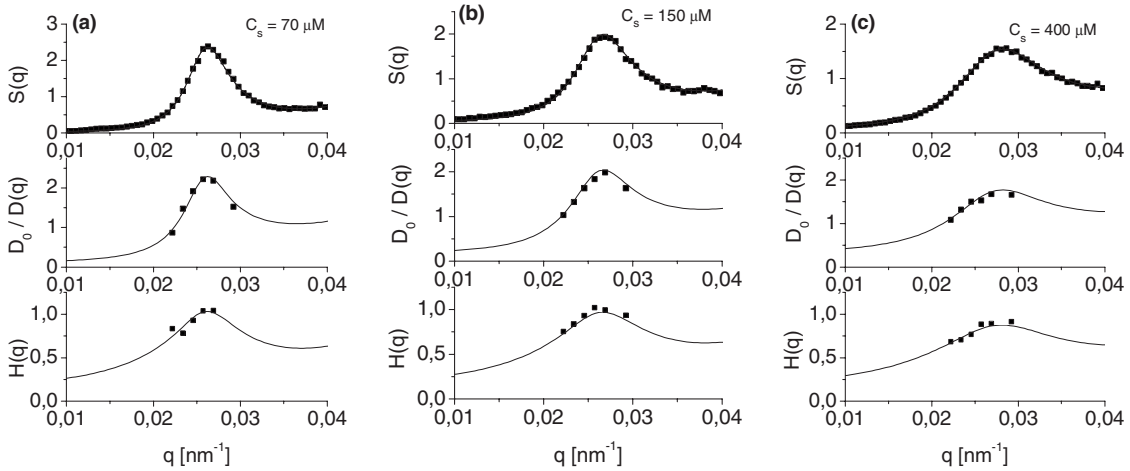

FIG. 3. [(a)–(c)] As in Fig. 2 but for more concentrated samples of series K. The salt concentrations C_s are indicated in the plots. Additional results on this series are available in the supplementary material (Ref. 46) in Fig. S2.

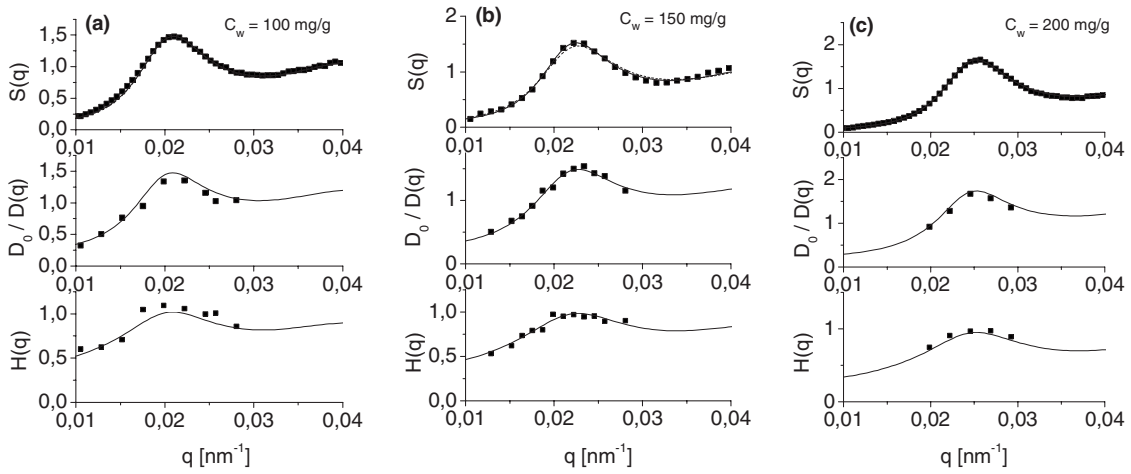

FIG. 4. [(a)–(c)] $S(q)$, $H(q)$, and the reciprocal of the normalized $D(q)$ for the samples of series C, where $C_s=50$ μM is kept constant and the colloid weight concentration is varied. The filled symbols represent the combined SAXS and XPCS data and the lines are the RY-fit results for $S(q)$ and the $\delta\gamma$-theory results for $H(q)$ and $D(q)$. The values of the silica weight concentration C_w are indicated in the plots. Parameters used in the calculations are given in Table I.

interesting point will be further discussed in the forthcoming article where we shall study the structure and dynamics of (partially) crystalline colloidal systems.

A corresponding set of results for the more concentrated samples of series K, where $\phi \approx 0.13-0.14$, is depicted in Fig. 3. The results for the samples of series C of fixed salinity $C_s=50$ μM and colloid concentration varying from 100 to 200 mg/g are depicted in Fig. 4.

The samples in series C could be maintained in the fluid state only for this comparatively large amount of added salt. According to Figs. 2–4, the undulations in $H(q)$ are growing with increasing ϕ and decreasing salt content, reflecting a similar behavior in $S(q)$. The peak positions of the two functions $S(q)$ and $H(q)$, and thus of $D_0/D(q)$, are all located at the same wave number q_m in accordance with the theoretical prediction. The diffusion function $D(q)$ attains its minimal value smaller than D_0 also at q_m. This value of the so-called cage-diffusion coefficient $D(q_m)$ describes the most slowly progressing (initial) decay of density fluctuations at a wavelength $2\pi/q_m$, quantifying the spatial extent of the dynamic cage of next-neighbor particles.

The good agreement between the experimental data for $D(q)$ and the $\delta\gamma$-scheme results, which is observed for practically all fluidlike samples in this study, is quite remarkable, considering that only the experimental structure factor peak height has been fitted. The agreement remains good even for the low-salinity samples, unless there are significant traces of crystalline order.

The low-salt systems in our study are precisely in the range of volume fractions where, for some charge-stabilized colloidal systems, extraordinarily small values of $H(q)$ have been reported,[8–11] which conflict with the predictions of the $\delta\gamma$-theory and Stokesian dynamics simulations.[6,23,24] In the present study and in many others,[6,18,19,22,23,48,49] such conflicting experimental results for $H(q)$ do not occur.

C. Salt-concentration dependence of various quantities

In analyzing series K, we have made an interesting observation. On trying to fit the SAXS scattered intensity in this series using the RMSA scheme, we noticed that the peak height of the RMSA intensity could not be enlarged enough to reach the experimental intensity peak values, regardless of the selected value of Z_{RMSA}. However, since the maximum in $S(q_m)$ as a function of the effective charge is larger in the RY than in the RMSA scheme, it was possible to fit the experimental data by the RY scheme without deviating from the experimentally given salt concentration. This finding highlights the advantage of the more accurate RY scheme over the RMSA in that certain more strongly coupled systems can be described consistently only by this more elaborate, partially self-consistent scheme.

In Fig. 5(a), we show the salt concentration dependence of Z_{RY} for all samples in series H and K. There is a certain ambiguity in the effective charge value for the largest salinity considered, since quite different values of the effective charge Z in the OMF pair potential can result in practically

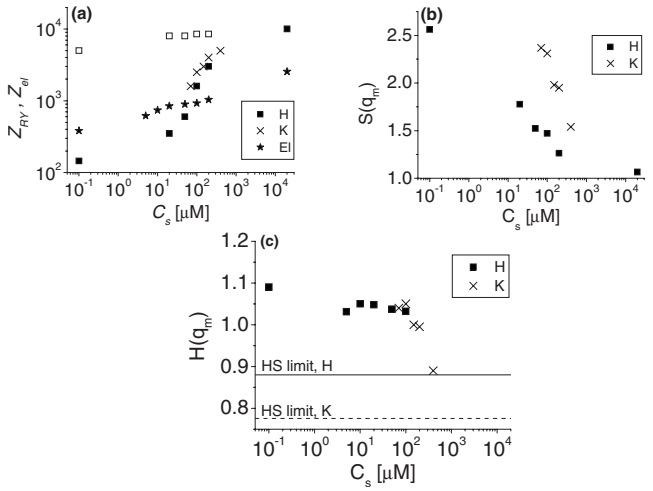

FIG. 5. (a) Fit values of the effective charge number Z_{RY} and the charge number Z_{el} (★) from the electrophoretic measurements, (b) maximum of the experimental $S(q)$, and (c) maximum of the $\delta\gamma$-scheme-fitted $H(q)$ of series H (■) and K (×) as a function of added salt concentration. In (a), the effective charge fit values from the high-charge branch of series H are also included (□). The HS limits of $H(q_m)$ for series H (solid line) and K (dashed line) are also shown in (c).

the same peak height in $S(q)$. The effective charge in series H and K grows steeply for salt concentrations where the number of added salt ions begins to exceed the number of surface-released counterions. This characterizes the transition regime from counterion-dominated to salt-ion dominated screening, where typically the most significant changes take place in quantities characterizing charge-stabilized suspensions.

It is interesting to note that nearly equally good fits to the static and dynamic scattering data can be achieved using an alternative branch of much higher effective charge values Z_{RY}. The charge values of this alternative branch are depicted in Fig. 5 as open squares. The salt-concentration dependence of these effective charges is much weaker since for such high charge values the salt-dominated concentration regime is not reached in the range of C_s values, as shown in Fig. 5. The occurrence of two well-separated branches of effective charge values with overall very similar $S(q)$ is not an artifact of the RY and RMSA schemes. It also follows, e.g., from Stokesian dynamics simulations. The physical origin of the two branches is the electrostatic screening effect of surface-released counterions. This effect grows with increasing Z and overcompensates eventually the influence of the growing pair potential contact value, leading to a $S(q_m)$ that passes through a maximum as a function of Z. For this reason, two well separated values of Z can give rise to overall very similar shapes of $S(q)$. To find out if the accessible range of effective charges of our colloidal system is sufficiently broad to include both branches, additional information is required.

For this reason electrophoretic light scattering measurements were performed on dilute samples (with $\phi \approx 1.25 \times 10^{-3}$) to get the electrophoretic mobility of the silica spheres as a function of C_s. From the measured mobility data, a rough estimate of the electrophoretic particle charge number Z_{el} was obtained using Henry's formula of single-sphere electrophoretic theory[1,50,51] by identifying the zeta potential with the electric potential on the sphere surface. The so-obtained values for Z_{el} are displayed as stars in Fig. 5(a). It can be expected and it was found indeed in recent electrophoresis studies on interacting colloidal particles that Z_{el} should not be dramatically different from the effective charge appearing in the OMF potential.[52,53] As one can notice from Fig. 5(a), the values of the high-charge branch for Z_{RY} are exceedingly larger than the electrophoretic charges.

We have also employed the RJM scheme[35] which provides values for the renormalized charge Z_{ren} as a function of the bare one. In comparison with the standard Poisson–Boltzmann cell model scheme for the effective charge by Alexander *et al.*,[37] the RJM has the advantage of being directly linked to the OMF pair potential in Eq. (6), and thus to Z_{RY}, and to maintain the validity of Eq. (7) in that the bare charge needs just to be replaced by the effective one. The effective charges derived from the two charge renormalization schemes are not very different from each other and reveal the same trends in their C_s and ϕ dependence.[30] For the present silica in DMF systems, we have found that the RJM renormalized charge is consistently smaller than $2000e$ even

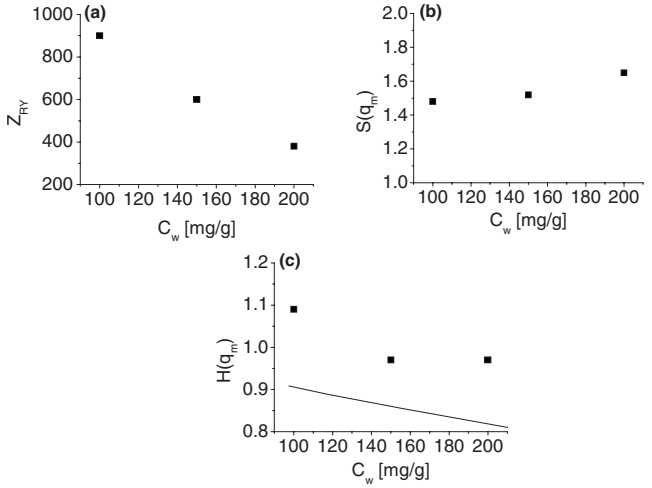

FIG. 6. Series C results (filled symbols) for (a) fit values of the effective charge Z_{RY}, (b) maximum of $S(q)$, and (c) maximum of $H(q)$ as a function of colloid concentration for a fixed added salt value of C_s=50 μM. The solid line in (c) represents the hard-sphere result, $H(q_m)=1-1.35\phi$.

in the saturation limit. Moreover, the renormalized charge shows a weak rise with increasing C_s similar to the electrophoretic charge in Fig. 5(a).

For all these reasons, we can rule out for our silica in DMF system the high-charge branch of RY values in Fig. 5(a). When performing extended structure factor fits using automatic routines, it is important to make sure which of the two branches each fitted result belongs to. For our silica in DMF system, we found that the low-charge branch should be used only, but this conclusion might not be valid any more for other systems.

We notice from Fig. 5(a) that Z_{el} is growing with increasing C_s, similar to the Z_{RY} of the lower branch. However, the rise in Z_{RY} is far more steep. An effective charge that grows with increasing C_s is also predicted by the charge renormalization schemes, and this can be explained by the enlarged screening by the salt leading to a smaller fraction of counterions which quasicondense on a colloid surface. While the ascent of the three discussed types of effective charges with increasing C_s is expected on physical grounds, we do not understand to date why Z_{RY} in Fig. 5(a) is rising far more steeply than the other two charges. To gain more insight into the interrelation of the effective colloid charges, charge regulation[54,55] and finite colloid concentration effects[56–59] should be considered. These effects have not been accounted for in our present discussion of Fig. 5(a). The salt-concentration dependence of $S(q_m)$ and $H(q_m)$ in series H and K is depicted in Figs. 5(b) and 5(c), respectively. The peak height in $S(q)$ shows the expected drop with increasing salt content, which reflects the corresponding loss in the particle correlations. Likewise, $H(q_m)$ approaches the corresponding hard-sphere value.

D. Colloid-concentration dependence of $H(q_m)$ and $S(q_m)$

The data for $H(q_m)$ in series H and K, depicted in Fig. 5(c) as a function of C_s, and likewise the data for the $H(q_m)$ of series C in Fig. 6(c), plotted as a function of the assumed

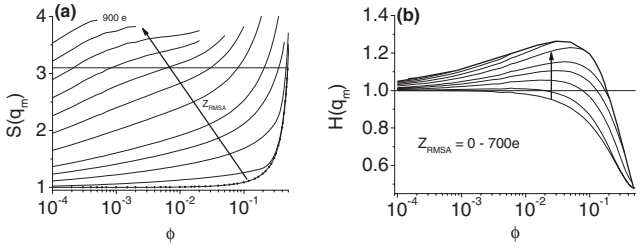

FIG. 7. $\delta\gamma$-RMSA values of (a) $S(q_m)$ and (b) of $H(q_m)$ at salt-free conditions calculated as a function of ϕ for various values of Z_{RMSA} as indicated (iso-Z_{RMSA} lines). The upper limiting contour line in (b) is derived from the cutoff condition $S(q_m) \leq 3.1$ for the onset of freezing. The solid isocharge lines are obtained from the lower branch of RMSA effective charge values. The solid arrows point to growing values of Z_{RMSA}.

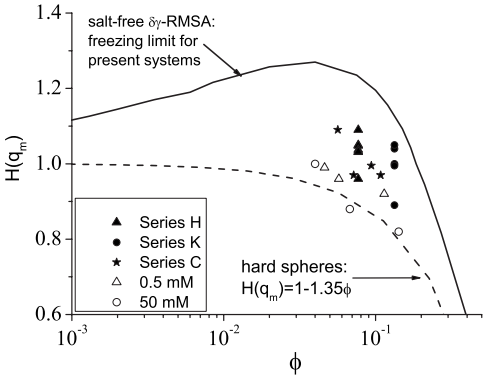

FIG. 8. Peak values of the hydrodynamic function $H(q)$ as a function of the colloid volume fraction ϕ. Included are our data for series H, K, and C. Further shown are XPCS data for 0.5 mM (△) and 50 mM (○) of added 1-1 electrolyte (Ref. 6). Lower dashed line: HSs. Upper solid line: Limiting freezing contour line for de-ionized fluid systems redrawn from Fig. 7.

colloid weight concentration C_w, are consistent with the generic ordering relation $H^{\mathrm{CS}}(q_m;\phi) > H^{\mathrm{HS}}(q_m;\phi)$ predicted both by the Stokesian dynamics simulations and the $\delta\gamma$-scheme. This relation expresses that the $H(q_m)$ of CSs is always higher than that of neutral HSs at the same ϕ.[6,23,24] The peak height value of HSs, which provides a lower boundary for charged colloidal spheres, is given to very good accuracy by

$$H(q_m) = 1 - 1.35\phi, \tag{10}$$

valid up to the freezing transition of HSs at ϕ=0.49 (Refs. 24 and 60). The exceptionally small values of $H(q)$ purportedly obtained in certain experiments on low-salt suspensions strongly violate this ordering relation.

The effective charge of series C depicted in Fig. 6(a) declines with increasing weight concentration when ϕ is increased from 0.056 to 0.108 (see Table I). This descent in Z_{RY} is compatible with a corresponding descent in the renormalized charge obtained from jellium model calculations for such a system of intermediate salinity.[30,35] The structure factor peak in series C increases only weakly with growing weight concentration [see Fig. 6(b)], since the effect of increasing ϕ is partially balanced by the decreasing effective charge.

At constant effective charge Z the highest value of $H(q_m)$ in a given system is attained, according to theory, for zero concentration of added salt. To fully explore the general behavior of $H(q_m)$ for fluid suspensions under salt-free conditions (C_s=0), we have used the $\delta\gamma$-scheme with the RMSA static structure factor input, which is numerically efficient enough to do such a detailed exploration in a reasonable amount of time. For each selected value of Z_{RMSA}, $H(q)$ was calculated and its maximum value $H(q_m)$ determined as a function of ϕ. In parallel, the maximum $S(q_m)$ of the RMSA-structure factor was calculated [see Fig. 7(a)] and plotted as a function of ϕ for selected effective charges. To limit ourselves to fluid systems, calculated values of $H(q_m)$ have been included in Fig. 7(b) only when the value of $S(q_m)$ is not larger than 3.1. This peak value has been reported as a reasonably good empirical Hansen–Verlet one-phase criterion[61] for the onset of colloid crystallization[62–65] for systems with long-range Yukawa-type pair interactions. The peak height value where crystallization sets in varies to some extent, depending on the range (softness) of the pair potential, from about 2.85 for HSs up to about 3.1 for more dilute samples of Yukawa-type particles with very long-range repulsion (zero-salinity systems). The range of the Yukawa-type pair potential, as quantified by κa, has also a bearing on whether crystallization in a more compact fcc phase or a less compact bcc phase takes place.[63,66,67]

Accepted fluidlike values of $H(q_m)$ have been plotted in Fig. 7(b) in the form of iso-Z_{RMSA} lines. By scanning through increasingly large values of Z_{RMSA}, for all of which $H(q_m)$ has been calculated, we have obtained the upper limiting contour line [see Fig. 7(b)] that restricts the values of $H(q_m)$ for fluid systems from above. This contour line consists of all isocharge line points for which $S(q_m)$=3.1. From below, the set of isocharge lines of $H(q_m)$ is limited by the curve describing the $H(q_m)$ of neutral HSs. Since the addition of salt reduces the degree of structural order, we can conclude that for any selected pair of ϕ and C_s values in the fluid regime, $H(q_m)$ is restricted in magnitude from above by the limiting contour line of zero-salt systems derived from the freezing criterion and from below by the zero-charge contour line of neutral HSs.

The maximum peak height attainable in our silica in DMF system, as predicted by the approximate $\delta\gamma$-RMSA scheme, is given by $H(q_m) \approx 1.27$ [see Fig. 7(b)]. Interestingly enough, this value can be reached only at a relatively low colloid concentration ($\phi \approx 0.04$) and for a moderate effective charge number of $Z_{\mathrm{RMSA}} \approx 400$. We can qualitatively rationalize the occurrence of this maximum by the following argumentation: for lower ϕ, where freezing of particles is achieved by increasing Z, the concentration of hydrodynamically interacting particles is too small to maximize, through spatial ordering, the collective motion of neighboring particles quantified by $H(q_m)$. For volume fraction values that are too large, the enhanced crowding of particles causes stronger near-field HIs to come into play with the effect of slowing down the cooperative motion of neighboring particles. The near-field hydrodynamic slowing down at higher ϕ can be so strong that $H(q_m)$ attains values smaller than one even for low-salt fluid systems.

In Fig. 8, finally, we have plotted the values of $H(q_m)$ obtained in the present experimental study (full symbols)

together with a set of values obtained from our recent XPCS study on fluorinated latex spheres[6] (open symbols). Furthermore, we have also included in this figure the upper limiting freezing contour line shown already in Fig. 7(b). All depicted experimental data fall within the region defined by this upper limiting curve and the hard-sphere curve. We would like to emphasize the fact that our results represent the properties of highly charged systems at very low salt conditions, in some cases very close to the crystalline state. In all cases the experimental points of $H(q_m)$ obtained for a given volume fraction at varying added salt concentration follow the simple rule: the lower C_s, the higher $H(q_m)$. No evidence of a short-time dynamics slower than expected from the OMF model calculations was found in the entire fluid range investigated in this study.

V. SUMMARY AND OUTLOOK

Using XPCS and SAXS measurements, the short-time diffusion functions $D(q)$ and $H(q)$ and the static structure factor $S(q)$ of charged silica spheres in DMF have been systematically studied in a broad range of colloid and salt concentrations. In contrast to earlier work, the explored systems cover the full fluid range from hard-sphere-like systems to the opposite extreme situation of de-ionized suspensions. The data for $D(q)$ and $H(q)$ obtained from the measurements in fluid-ordered systems could be consistently described by the $\delta\gamma$-scheme calculations. No signature of any unusually small $H(q)$ values was found, even for low-salt systems close to the freezing line, as reported by other authors.[10,11] Extensive calculations of the peak values $H(q_m)$ of the hydrodynamic function of fluid systems, characterized by the empiric criterion $S(q_m)<3.1$, in a broad range of ϕ and Z values have revealed a characteristic region where all values for $H(q_m)$ can be found. This type of analysis can be of help in the interpretation of existing experimental data and in identifying conditions where either hydrodynamic hindrance or enhancement of collective diffusion may be found. The upper limiting contour line in Fig. 7(b) does not depend critically on the selected peak value of the freezing criterion. A change in the peak value from 3.1 to 2.9 leads to a small shift in the contour line only.

In the present study, only systems without noticeable indications of crystallization have been considered and interpreted in terms of theoretical schemes designed for fluid systems. Partially and fully crystalline suspensions require a special analysis of the measured scattering functions by methods which account for the long-range particle ordering. Such an analysis for silica spheres in DMF is in progress and will be communicated in a future publication.

In addition to the study of $H(q)$ and $S(q)$, we have also investigated the salt and colloid concentration dependence of the effective charge numbers Z_{RY} and Z_{el} obtained, respectively, from the RY static structure factor fit based on the OMF pair potential and from single-particle electrophoresis measurements. There exists a second branch of high-charge values for Z_{RY} which leads to equally good fits of the experimental data. For the present silica in DMF systems, however, this branch is ruled out in view of independent experimental and theoretical results, but it might be relevant to other systems. The general trends in the C_s and ϕ-dependence of the physical branch values of Z_{RY} conform to those of Z_{el} and to the renormalized particle charge obtained from the RJM. However, the rise in Z_{RY} with increasing salt content is much steeper, an observation which we cannot explain to date. A deeper understanding of these effective charges and their interrelations will require a detailed theoretical and experimental analysis, involving the consideration of charge-regulation effects[54,55] on the silica surfaces and colloid correlation effects, in particular, when the electrophoretic mobility is considered. Notwithstanding the progress made in our understanding of structural and electrohydrodynamic effects in suspensions of interacting charged colloidal particles,[52,53,56–59] a lot more needs to be learned about the various types of static and dynamic effective charges. This is left to future work.

ACKNOWLEDGMENTS

This work has been supported by the Deutsche Forschungsgemeinschaft (Grant No. SFB-TR6, Project Sec. B2). Part of this work was done within the framework of the "SoftComp" Network of Excellence (Grant No. S080118). A.J.B. acknowledges financial support from FONCYT (Grant No. OICT 2005-33691) and SeCyT-UNC.

[1] W. B. Russel, D. A. Saville, and W. R. Schowalter, *Colloidal Dispersions* (Cambridge University Press, Cambridge, 1989).
[2] P. N. Pusey, in *Liquids, Freezing and Glass Transition, Les Houches Sessions 1989*, edited by J.-P. Hansen, D. Levesque, and J. Zinn-Justin (North-Holland, Amsterdam, 1991), pp. 763–942.
[3] G. Nägele, Phys. Rep. **272**, 215 (1996).
[4] J. K. G. Dhont, *An Introduction to Dynamics of Colloids* (Elsevier, New York, 1996).
[5] A. J. Banchio, J. Gapinski, A. Patkowski, W. Häussler, A. Fluerasu, S. Saccana, P. Holmqvist, G. Meier, M. P. Lettinga, and G. Nägele, Phys. Rev. Lett. **96**, 138303 (2006).
[6] J. Gapinski, A. Patkowski, A. J. Banchio, P. Holmqvist, G. Meier, M. P. Lettinga, and G. Nägele, J. Chem. Phys. **126**, 104905 (2007).
[7] A. Robert, Ph.D. thesis, Université Joseph Fourier, 2001.
[8] D. O. Riese, W. L. Vos, G. H. Wegdam, F. J. Poelwijk, D. Abernathy, and G. Grübel, Phys. Rev. E **61**, 1676 (2000).
[9] G. Grübel, D. Abernathy, D. O. Riese, W. L. Vos, and G. H. Wegdam, J. Appl. Crystallogr. **33**, 424 (2000).
[10] T. Autenrieth, A. Robert, J. Wagner, and G. Grübel, J. Appl. Crystallogr. **40**, 250 (2007).
[11] D. O. Riese, G. H. Wegdam, W. L. Vos, R. Sprik, D. Fenistein, J. H. H. Bongaerts, and G. Grübel, Phys. Rev. Lett. **85**, 5460 (2000).
[12] C. W. J. Beenakker and P. Mazur, Physica A **126**, 349 (1984).
[13] C. W. J. Beenakker and P. Mazur, Phys. Lett. **98**A, 22 (1983).
[14] C. W. J. Beenakker, Ph.D. thesis, University of Leiden, 1984.
[15] U. Genz and R. Klein, Physica A **171**, 26 (1991).
[16] G. Nägele, B. Steininger, U. Genz, and R. Klein, Phys. Scr. **T55**, 119 (1994).
[17] G. Nägele, B. Mandl, and R. Klein, Prog. Colloid Polym. Sci. **98**, 117 (1995).
[18] L. F. Rojas, R. Vavrin, C. Urban, J. Kohlbrecher, A. Stradner, F. Scheffold, and P. Schurtenberger, Faraday Discuss. **123**, 385 (2003).
[19] L. F. Rojas, Ph.D. thesis, University of Fribourg, 2004.
[20] J. P. Hansen and J. B. Hayter, Mol. Phys. **46**, 651 (1982).
[21] F. J. Rogers and D. A. Young, Phys. Rev. A **30**, 999 (1984).
[22] J. Gapinski, A. Wilk, A. Patkowski, W. Häussler, A. J. Banchio, R. Pecora, and G. Nägele, J. Chem. Phys. **123**, 054708 (2005).
[23] A. J. Banchio, J. Gapinski, A. Patkowski, W. Häussler, A. Fluerasu, S. Saccana, P. Holmqvist, G. Meier, M. P. Lettinga, and G. Nägele, Phys. Rev. Lett. **96**, 138303 (2006).
[24] A. J. Banchio and G. Nägele, J. Chem. Phys. **128**, 104903 (2008).

[25] A. J. Banchio, M. G. McPhie, and G. Nägele, J. Phys.: Condens. Matter **20**, 404213 (2008).
[26] R. B. Jones and P. N. Pusey, Annu. Rev. Phys. Chem. **42**, 137 (1991).
[27] J. W. Verwey and J. T. G. Overbeek, *Theory of the Stability of Lyotropic Colloids* (Elsevier, New York, 1948).
[28] W. B. Russel and D. W. Benzing, J. Colloid Interface Sci. **83**, 163 (1981).
[29] R. Denton, Phys. Rev. E **62**, 3855 (2000).
[30] E. Trizac, L. Bocquet, M. Aubouy, and H. H. von Grünberg, Langmuir **19**, 4027 (2003).
[31] B. Beresford-Smith, D. Y. Chan, and D. J. Mitchell, J. Colloid Interface Sci. **105**, 216 (1985).
[32] L. F. Rojas, C. Urban, P. Schurtenberger, T. Gisler, and H. H. von Grünberg, Europhys. Lett. **60**, 802 (2002).
[33] A. Diehl and Y. Levin, J. Chem. Phys. **121**, 12100 (2004).
[34] W. L. Hsin, T. Y. Wang, Y. J. Sheng, and H. K. Tsao, J. Chem. Phys. **121**, 5494 (2004).
[35] S. Pianegonda, E. Trizac, and Y. Levin, J. Chem. Phys. **126**, 014702 (2007).
[36] A. Torres, G. Tellez, and R. van Roij, J. Chem. Phys. **128**, 154906 (2008).
[37] S. Alexander, P. M. Chaikin, P. Grant, G. J. Morales, and P. Pincus, J. Chem. Phys. **80**, 5776 (1984).
[38] M. J. Stevens, M. L. Falk, and M. O. Robbins, J. Chem. Phys. **104**, 5209 (1996).
[39] G. Nägele, *The Physics of Colloidal Soft Matter* (Polish Academy of Sciences Publication, Warsaw, 2004).
[40] K. Osseo-Asare and F. J. Arriagada, Colloids Surf. **50**, 321 (1990).
[41] F. J. Arriagada and K. Osseo-Asare, J. Colloid Interface Sci. **211**, 210 (1999).
[42] H. Giesche, J. Eur. Ceram. Soc. **14**, 205 (1994).
[43] J. Chang, P. Lesieur, M. Delsanti, L. Belloni, C. Bonnet-Gonnet, and B. Cabane, J. Phys. Chem. **99**, 15993 (1995).
[44] T. Thurn-Albrecht, F. Zontone, G. Grübel, W. Steffen, P. Müller-Buschbaum, and A. Patkowski, Phys. Rev. E **68**, 031407 (2003).
[45] http://www.esrf.eu.
[46] See EPAPS Document No. E-JCPSA6-130-009908 for the plots of additional experimental results of $S(q)$, $D(q)$, and $H(q)$. For more information on EPAPS, see http://www.aip.org/pubservs/epaps.html.
[47] S. H. Behrens and D. G. Grier, J. Chem. Phys. **115**, 6716 (2001).
[48] A. P. Philipse and A. Vrij, J. Chem. Phys. **88**, 6459 (1988).
[49] W. Härtl, Ch. Beck, and R. Hempelmann, J. Chem. Phys. **110**, 7070 (1999).
[50] R. J. Hunter, *Zeta Potential in Colloid Science: Principles and Applications* (Academic, New York, 1981).
[51] H. Ohshima, *Theory of Colloid and Interfacial Electric Phenomena, Interface Science and Technology* (Elsevier, New York, 2006), Vol. 12.
[52] V. Lobaskin, B. Dünweg, C. Holm, M. Medebach, and T. Palberg, Phys. Rev. Lett. **98**, 176105 (2007).
[53] H. Reiber, T. Köller, T. Palberg, F. Carrique, E. R. Ruiz Reina, and R. Piazza, J. Colloid Interface Sci. **309**, 315 (2007).
[54] T. Gisler, S. F. Schulz, M. Borkovec, H. Sticher, P. Schurtenberger, B. D'Aguanno, and R. Klein, J. Chem. Phys. **101**, 9924 (1994).
[55] E. Lee, C.-H. Fu, and J.-P. Hsu, J. Colloid Interface Sci. **250**, 327 (2002).
[56] T. Araki and H. Tanaka, Europhys. Lett. **82**, 18004 (2008).
[57] K. Kim, Y. Nakayama, and R. Yamamoto, Phys. Rev. Lett. **96**, 208302 (2006).
[58] M. G. McPhie and G. Nägele, J. Chem. Phys. **127**, 034906 (2007).
[59] L. F. Rojas-Ochoa, Phys. Rev. Lett. **100**, 178304 (2008).
[60] A. J. Banchio, G. Nägele, and J. Bergenholtz, J. Chem. Phys. **111**, 8721 (1999).
[61] J.-P. Hansen and L. Verlet, Phys. Rev. **184**, 151 (1969).
[62] K. Kremer, M. O. Robbins, and G. S. Grest, Phys. Rev. Lett. **57**, 2694 (1986).
[63] M. O. Robbins, K. Kremer, and G. S. Grest, J. Chem. Phys. **88**, 3286 (1988).
[64] H. Löwen, T. Palberg, and R. Simon, Phys. Rev. Lett. **70**, 1557 (1993).
[65] D. C. Wang and A. P. Gast, J. Phys.: Condens. Matter **11**, 10133 (1999).
[66] A.-P. Hynninen and M. Dijkstra, J. Phys.: Condens. Matter **15**, S3557 (2003).
[67] E. B. Sirota, H. D. Ou-Yang, S. K. Sinha, P. M. Chaikin, J. D. Axe, and Y. Fujii, Phys. Rev. Lett. **62**, 1524 (1989).